RSC Advances

PAPER

View Article Online
View Journal | View Issue

Open Access Article. Published on 05 May 2022. Downloaded on 3/3/2026 10:20:57 AM.
This article is licensed under a Creative Commons Attribution-NonCommercial 3.0 Unported Licence.

Check for updates

Cite this: *RSC Adv.*, 2022, **12**, 13645

Fabrication of gelatin Bi_2S_3 capsules as a highly sensitive X-ray contrast agent for gastrointestinal motility assessment *in vivo*†

Ya Wen,‡[a] Wang Zhu,‡[b] Xuejun Zhang*[a] and Shao-Kai Sun *[a]

Received 15th February 2022
Accepted 13th April 2022

DOI: 10.1039/d2ra00993e

rsc.li/rsc-advances

Tiny $BaSO_4$ rod-based X-ray imaging is the most frequently-used method for clinical diagnosis of gastrointestinal motility disorders. The $BaSO_4$ rods usually have a small size to pass through the gastrointestinal tract smoothly, but suffer from unavoidably low sensitivity. Herein, we developed Bi_2S_3 capsules as a high-performance X-ray contrast agent for gastrointestinal motility assessment for the first time. The Bi_2S_3 capsules were synthesized by the encapsulation of commercial Bi_2S_3 powder into commercial gelatin capsules and subsequent coating of ultraviolet-curable resin. The prepared Bi_2S_3 capsules showed excellent biocompatibility *in vitro* and *in vivo* and superior X-ray attenuation ability due to the large atomic number and high K-edge value of Bi. The developed Bi_2S_3 capsules can serve as a small but highly sensitive X-ray contrast agent to quantitatively assess gastrointestinal motility in a vincristine-induced gastrointestinal motility disorder model *in vivo* by X-ray, CT and spectral CT imaging successfully, solving the intrinsic drawbacks of clinically used $BaSO_4$.

Introduction

Gastrointestinal motility disorders are common complications of a variety of diseases, such as diabetes, obesity, hypertension, and adverse reactions during treatment with chemotherapy drugs like vincristine, which may lead to constipation or diarrhea.[1–5] For instance, nearly one-third of patients receiving vincristine treatment will have symptoms such as constipation and paralytic intestinal obstruction induced by autonomic nervous system dysfunction, which can last for several months and seriously affects the patient's quality of life and treatment compliance.[6–11] Eventually, gastrointestinal motility disorders lead to the decreased absorption of nutrients and changes in the intestinal barrier function and strongly affect the normal function of the body. Thus, timely and accurate assessment of gastrointestinal function has far-reaching clinical significance.

Non-invasive imaging examinations, such as radiopaque marker tests, radionuclide scintigraphy and wireless motility capsules,[12] have been frequently used in the diagnosis of various gastrointestinal diseases due to the advantage of non-invasiveness.[13,14] Among these clinical imaging technologies, radiopaque marker test[15] owns the merits of simple operation, easy analysis and low cost.[16] The use of the first radiopaque agent most likely dates back to 1896, when $BaSO_4$ was used to study gastrointestinal motility of animals[17] and various morphologies of $BaSO_4$ agents have been developed to meet the requirement of different diseases during the past decades.[18–21] Currently, for gastrointestinal motility assessment in clinic, the patients orally take 2 capsules (containing 20 $BaSO_4$ rods) after breakfast on the day of examination. Then the whole gut transit time was evaluated through observing the change of the position and the number of $BaSO_4$ rods at different time points by X-ray imaging.[15,22–25] To satisfy the need of normal gastrointestinal transport, $BaSO_4$ rods are usually small in size. While size is a double-edged sword, which results in inherent low sensitivity of $BaSO_4$ rods and makes it difficult to definite their position in gastrointestinal tract. However, $BaSO_4$ rods have been used for gastrointestinal motility assessment for several decades, and there were few new X-ray contrast agents reported up to now. Thus, it is our great desire to develop a highly sensitive and biocompatible X-ray contrast agent for gastrointestinal motility assessment.

Besides X-ray imaging, X-ray computed tomography (CT) imaging, which is capable of three-dimensional reconstruction, is increasingly used in gastrointestinal examinations, and provides abundant diagnosis information that X-ray imaging fails to give.[26–28] Especially, the principle of spectral CT is to collect two data sets from the same anatomical location using different kilovolt peaks, possesses differentiation ability towards materials with different absorption under various X-ray energies. It can reduce image artifacts, distinguish tissue components, and improve the contrast effect of high atomic

[a]*Department of Medical Imaging, Tianjin Medical University, Tianjin 300203, China. E-mail: zhangxj@tmu.edu.cn; shaokaisun@tmu.edu.cn*

[b]*Department of Radiographic Center, Wuhan Children's Hospital, Tongji Medical College of Huazhong University of Science and Technology, Wuhan, 430015, China*

† Electronic supplementary information (ESI) available. See https://doi.org/10.1039/d2ra00993e

‡ These authors contributed equally to the work.

© 2022 The Author(s). Published by the Royal Society of Chemistry

Open Access Article. Published on 05 May 2022. Downloaded on 3/3/2026 10:20:57 AM.
This article is licensed under a Creative Commons Attribution-NonCommercial 3.0 Unported Licence.

number elements-based contrast agents to surrounding tissues, which provides a promising way to assess gastrointestinal motility.[5,29–34] Similar to X-ray imaging, high-performance contrast agents are also the key to sensitive and accurate evaluation of gastrointestinal motility by CT and spectral CT. However, $BaSO_4$ and iodine-based small molecules commonly used clinically are not suitable for CT and spectral CT imaging due to the low K-edge energies of Ba and I and relatively poor X-ray attenuation ability.[5,17,35]

Bi has the highest atom number among non-radioactive elements ($Z = 83$)[36–38] and possesses an outstanding X-ray attenuation coefficient (Bi: 5.74, Au: 5.16, Pt: 4.99, and Ta: 4.3 $cm^2\ g^{-1}$ at 100 keV).[39] In addition, Bi is the cheapest element among the heavy metal elements suitable for X-ray imaging. Besides, Bi is a highly biocompatible element,[36] and many Bi-based compounds, known as "bismuth therapy",[40–43] have served as drugs for gastrointestinal diseases for more than three hundred years.[44] In the past decades, various Bi-based nanomaterials, such as Bi,[44–47] Bi_2O_3,[48–51] Bi_2Se_3,[52–54] Bi_2S_3,[55–58] have been developed as the new generation of X-ray contrast agents for diagnosis of various diseases. However, a Bi-based contrast agent for gastrointestinal motility assessed by X-ray, CT and spectral CT has not been reported so far (Scheme 1).

Herein, we proposed a highly sensitive method for gastrointestinal transmission assessment using Bi_2S_3 capsules by X-ray, CT, and spectral CT imaging *in vivo*. The radiopaque capsules rather than water-soluble nanoparticles are needed in assessment gastrointestinal tract transmission. Commercial Bi_2S_3 powder was selected as Bi precursor due to its excellent chemical stability, high content of Bi element, good X-ray absorption capacity and low price. It was encapsulated in commercial gelatin capsules and then coated with ultraviolet-curable resin to generate the uniform Bi_2S_3 capsules. The prepared Bi_2S_3 capsules had good stability and superior X-ray (especially high-energy X-ray) attenuation ability compared to $BaSO_4$. High sensitive gastrointestinal transmission assessment by X-ray imaging was successfully achieved using Bi_2S_3 capsules, which was much more sensitive than that using $BaSO_4$. Besides, Bi_2S_3 capsules were also employed in CT and spectral CT imaging *in vivo*, and real-time, sensitive, and high-spatial resolution visualization of the gastrointestinal motility was realized, providing abundant three mention information. *In vitro* and *in vivo* toxic studies proved the excellent biocompatibility of Bi_2S_3 capsules. To the best of our knowledge, it was the first time that a Bi-based contrast agent was used to evaluate gastrointestinal motility, which showed great potential as an alternative to clinic $BaSO_4$.

Results and discussion

Synthesis and characterization of Bi_2S_3 capsules

The commercial Bi_2S_3 powder with tiny size was used as the precursor for the synthesis of Bi_2S_3 capsules to achieve high imaging sensitivity (Fig. 1A and S2†). The X-ray diffraction pattern indicated the Bi_2S_3 belonged to the orthorhombic system (Fig. 1C).[59,60] Despite the size of Bi_2S_3 powder showed the evident variability on micrometer scale (Fig. S3†), it was uniform on millimeter scale, which was sufficient to produce uniform Bi_2S_3 capsules (Fig. 1B). Synthesizing biomaterials with biocompatible macromolecules can improve their biosafety, so we used gelatin capsules as a carrier to prepare Bi_2S_3 capsules[61,62] (Fig. 1D). The resin coating was essential to ensure the stability of Bi_2S_3 capsules in gastrointestinal tract environments. The synthesized Bi_2S_3 capsules had a uniform size with 3 mm in diameter and 8 mm in length and there were 25 mg Bi_2S_3 in each capsule. Thus, the synthesis of Bi_2S_3 capsules was extremely and reproducible.

To investigate the stability of Bi_2S_3 capsules in stimulated gastrointestinal tract environments, the Bi_2S_3 capsules were immersed into diluted HCl solution (pH = 1) and artificial small

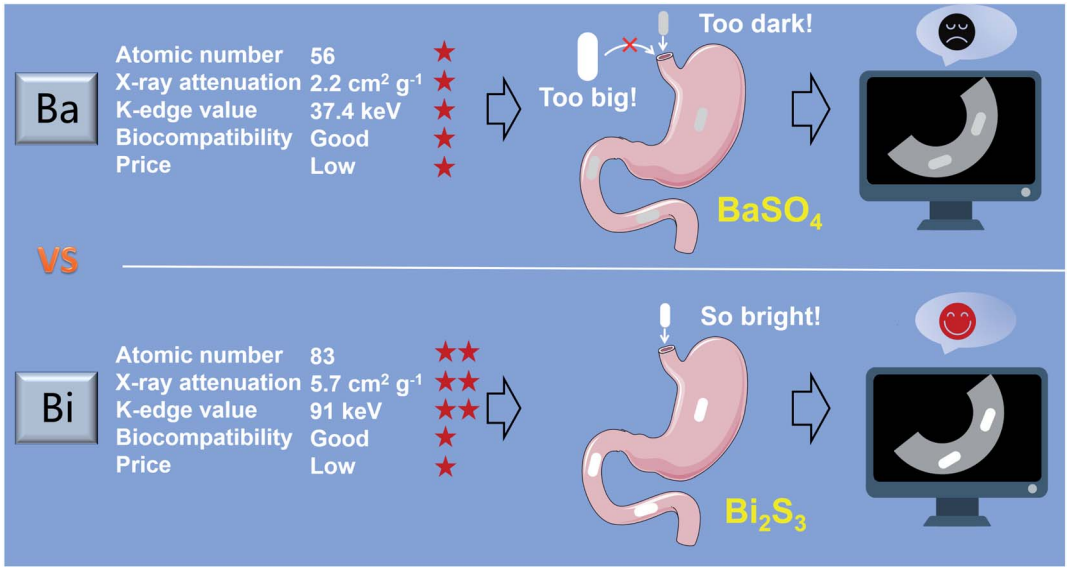

Scheme 1 Schematic illustration of synthesis of Bi_2S_3 capsules as a X-ray contrast agent for gastrointestinal tract visualization *in vivo*.

 © 2022 The Author(s). Published by the Royal Society of Chemistry

Open Access Article. Published on 05 May 2022. Downloaded on 3/3/2026 10:20:57 AM.
This article is licensed under a Creative Commons Attribution-NonCommercial 3.0 Unported Licence.

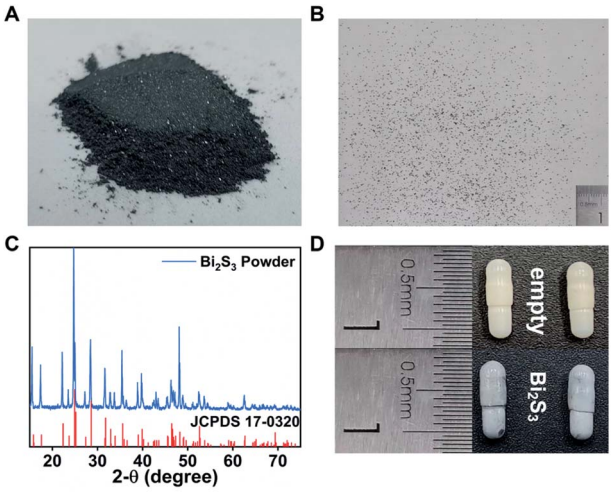

Fig. 1 Characterization of Bi_2S_3 powder and capsules. (A) The photo of commercial Bi_2S_3 powder. (B) The photo of dispersed Bi_2S_3 power in millimeter scale. (C) X-ray diffraction pattern of Bi_2S_3 powder. (D) The photo of empty gelatin capsule (upper panel) and Bi_2S_3 capsules (lower panel).

intestinal fluid for 12 h. The morphology of the capsule had no obvious change, and there was no leakage of Bi_2S_3 power. The results indicated the Bi_2S_3 capsules could resist the gastrointestinal tract environments and keep stable for potential applications (Fig. S4†).

X-ray, CT and spectral CT imaging *in vitro*

To compare the X-ray absorbance ability of Bi_2S_3 with clinical $BaSO_4$ and iohexol *in vitro*, different suspensions were synthesized by dispersing Bi_2S_3, $BaSO_4$ and iohexol power into alginate–Ca^{2+} hydrogel. In addition, $BaSO_4$ and iohexol capsules were also prepared according to the synthesis procedures of Bi_2S_3 capsules. X-ray images of various suspensions indicated their brightness increased with the increase of concentrations of radiopaque elements (Bi, Ba, and I), and the Bi_2S_3 suspension showed a higher brightness than $BaSO_4$/iohexol suspensions at an equivalent mass or molar concentrations of radiopaque elements (Fig. S5†). And the Bi_2S_3 capsule was much brighter than that of $BaSO_4$ and iohexol capsule (Fig. S6†). It should be noted that there was serious interference from food in gastrointestinal tract imaging, and iohexol was used to visualize the gastrointestinal tract profile sometimes, so the imaging ability of the capsules should also be evaluated in the presence of food or iohexol. These capsules all showed much higher brightness than food or iohexol solution visually, and the boundary between capsules and surrounding food or iohexol can be seen obviously (Fig. S7†). Quantitative analysis indicated Bi_2S_3 capsules exhibited the highest brightness among them. These results indicated Bi_2S_3 capsules had great potential in serving as a superior X-ray contrast agent.

In CT imaging, with the increasing concentrations of radiopaque elements, the CT images of Bi_2S_3 suspensions were brighter than the corresponding images of $BaSO_4$ and iohexol suspensions at various tube voltages (80, 100, 120, and 140 kV). Meanwhile, the Hounsfield unit (HU) values linearly increased under the same voltage for Bi_2S_3, $BaSO_4$ and iohexol suspensions and capsules in a concentration dependent manner and the slope discrepancy among Bi_2S_3, $BaSO_4$ and iohexol became more and more distinct along with the increasing tube voltage from 80 to 140 kV (Fig. 2A–D, S8 and S9†). The CT imaging ability of Bi_2S_3 capsules in food and iohexol were also investigated, and the results confirmed that Bi_2S_3 capsules had the best CT imaging performance even in the high background induced by food and iohexol (Fig. S10A and S11†). In order to study the feasibility of spectral CT imaging using Bi_2S_3, monochromatic images of Bi_2S_3, $BaSO_4$, and iohexol suspensions were obtained (Fig. 3A–C and S12†). Under each X-ray energy, there is a linear relationship between HU value and concentration of contrast agents. At low X-ray energies (40–50 keV), the HU values of $BaSO_4$ and iohexol suspensions were higher than those of Bi_2S_3 suspensions. As the tissues were mainly composed of low atomic number elements, they showed similar X-ray absorption properties to $BaSO_4$ or iohexol and also have a relatively high X-ray absorption at low X-ray energies. Hence it is useless to perform spectral CT imaging using $BaSO_4$ or iohexol as contrast agents at low X-ray energies. When the energy is larger than about 60 keV, the HU values of Bi_2S_3 suspensions became higher than those of $BaSO_4$ and iohexol suspensions, and the slope (HU value per unit concentration) difference between Bi_2S_3 suspensions and $BaSO_4$/iohexol suspensions becomes more and more obvious when monochromatic energy increased.

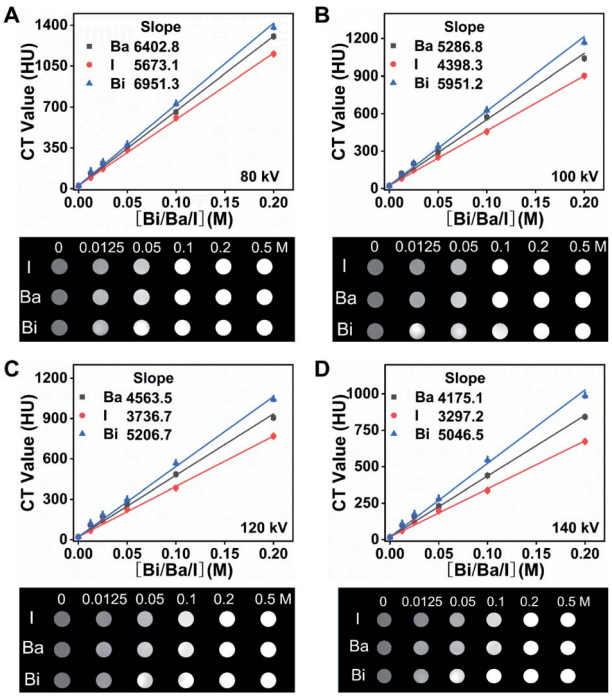

Fig. 2 HU curves and CT images of Bi_2S_3, $BaSO_4$ and iohexol suspensions with different concentrations of radiopaque elements (0.0125, 0.025, 0.05, 0.1, and 0.2 M Bi, Ba or I) at (A) 80 kV, (B) 100 kV, (C) 120 kV, (D) 140 kV.

Open Access Article. Published on 05 May 2022. Downloaded on 3/3/2026 10:20:57 AM.
This article is licensed under a Creative Commons Attribution-NonCommercial 3.0 Unported Licence.

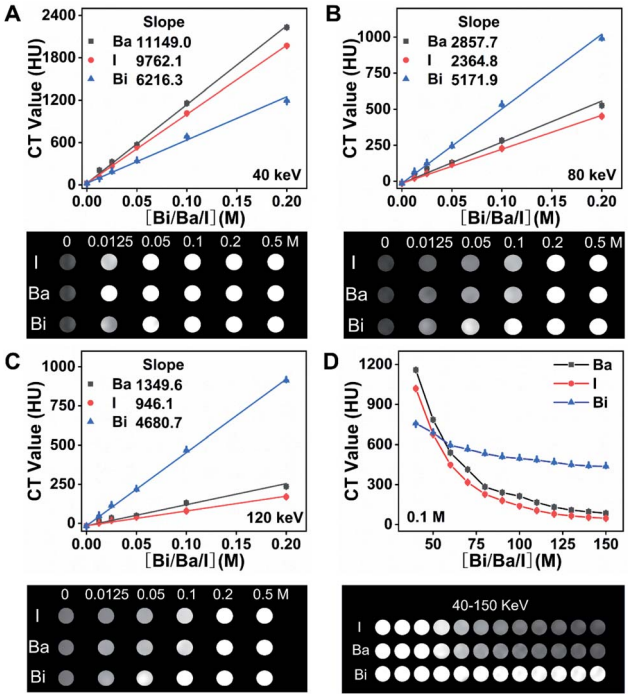

Fig. 3 HU curves and spectral CT images of Bi_2S_3, $BaSO_4$ and iohexol suspensions at different concentrations of radiopaque elements (0.0125, 0.025, 0.05, 0.1, and 0.2 M Bi, Ba or I) at (A) 40 keV, (B) 80 keV, (C) 120 keV. (D) Spectral CT HU curves and images of Bi_2S_3, $BaSO_4$ and iohexol (0.1 M Bi, Ba or I) at different monochromatic energies.

Compared with the sharp decrease of the HU value of $BaSO_4$ and iohexol suspensions with the increase of monochromatic energy, Bi_2S_3 suspensions exhibit relatively stable HU value due to the high K-edge energy of Bi (91 keV) (Fig. 3D). These results indicated Bi_2S_3 exhibited excellent spectral CT imaging ability at high X-ray energies. Then we evaluated the spectral CT imaging ability of Bi_2S_3 capsule. Similar to Bi_2S_3 suspension, Bi_2S_3 capsule showed better CT imaging performance when the energy increased from 80 keV to 160 keV, and the energies were higher, the performance was better (Fig. 4). In the presence of food, three kinds of capsules all showed a good contrast effect, and the boundary between capsules and food was very clear, but a quantitative analysis indicated the HU value of Bi_2S_3 capsule

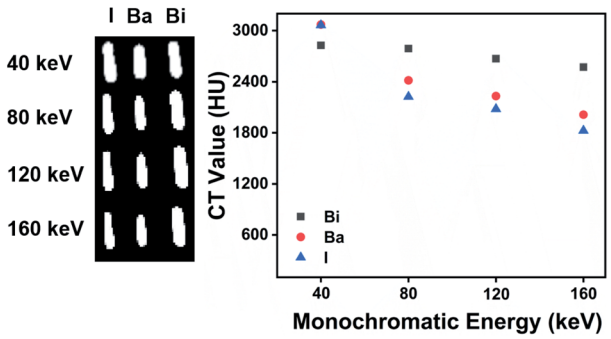

Fig. 4 Spectral CT images and HU values of full of Bi_2S_3, $BaSO_4$ and iohexol capsules.

was the highest (Fig. S10B†). In the presence of iohexol, it is hard to distinguish capsules from iohexol only if the concentration of iohexol was very low (5 mg mL^{-1}) at low X-ray energies. However, when the X-ray energies were larger, the contrast of HU values of capsules and iohexol solution became significant, and the boundary between them can be seen obviously (Fig. S13†). It should be noted the size of Bi_2S_3 capsule kept the same in spectral CT images at various X-ray energies while the size of $BaSO_4$ capsule became smaller along with the increase of X-ray energies. Besides, the HU values of Bi_2S_3 capsule were higher than those of $BaSO_4$ capsule at various X-ray energies. These results demonstrated Bi_2S_3 capsule can serve as a spectral CT imaging contrast agent with high sensitivity, which was capable of minimizing the interference of surrounding substance.

Cytotoxicity assessment

The cytotoxicity of Bi_2S_3 capsules was evaluated by a standard MTT test. Firstly, Bi_2S_3 capsules were dispersed in various media (ultrapure water, phosphate buffered saline (PBS) solution (pH = 7.4) and diluted hydrochloric acid (pH = 1)) for 24 h, and the leaching solutions were acquired by removing the capsules. Then, 3T3-L1 cells were incubated with various leach solutions for 12 h and the cell viabilities were determined. The results indicated Bi_2S_3 capsule leach solutions had little influence on the proliferation of 3T3-L1 cells, and the cell viability remained above 80% (Fig. S14†), indicating the low cytotoxicity of Bi_2S_3 capsules.

In vivo toxicity of Bi_2S_3 capsule

To investigate the *in vivo* toxicity of Bi_2S_3 capsules, hematoxylin and eosin (H&E) staining analysis of the main organs (heart, liver, spleen, lung, kidney, and the intestinal tract) at different time points was carried out after oral administration of three Bi_2S_3 capsules (Fig. S15†). H&E staining results demonstrated there were no obvious histopathological damages in major organs of rats after the treatment of Bi_2S_3 capsules, further proving their good biocompatibility.

Gastrointestinal transmission assessment by X-ray imaging *in vivo*

Based on the excellent X-ray absorption ability of Bi_2S_3 capsules, we investigated the feasibility of gastrointestinal transmission assessment using Bi_2S_3 capsules by X-ray imaging on vincristine-induced gastrointestinal motility disorder models. Paralytic ileus caused by vincristine can be prevented/treated by CB1 antagonists, such as AM251.[63]

The rats were divided into three groups including a control group, vincristine-treated group and vincristine & AM251-treated group (n = 8 in each group). After oral administration of three Bi_2S_3 capsules, the X-ray imaging was carried out at different time points (0 min, 5 min, 2 h, 4 h, 8 h, and 10 h) (Fig. 5A–C). For all the groups of rats, three Bi_2S_3 capsules can be seen clearly in esophagus and stomach after the administration of capsules in X-ray imaging, and then the capsules moved into small intestinal gradually. At 2 h, the rats were orally

 © 2022 The Author(s). Published by the Royal Society of Chemistry

Open Access Article. Published on 05 May 2022. Downloaded on 3/3/2026 10:20:57 AM.
This article is licensed under a Creative Commons Attribution-NonCommercial 3.0 Unported Licence.

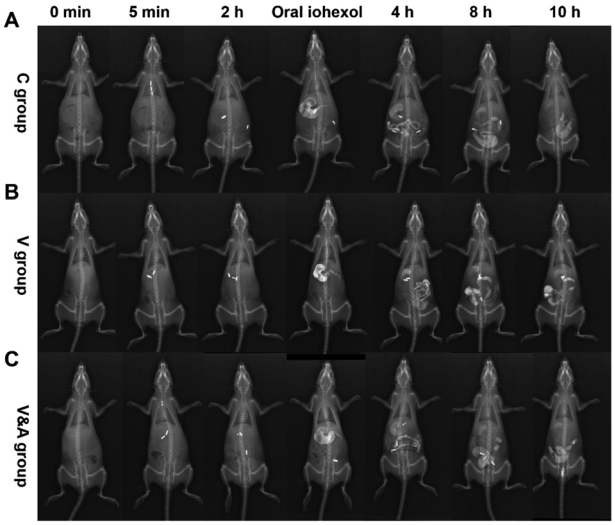

Fig. 5 X-ray images of rats after various treatments at different time points (0 min, 5 min, 2 h, 4 h, 8 h, 10 h) *in vivo*. (A) Control group (C group), (B) vincristine-treated group (V group), (C) vincristine & AM251 treated group (V&A group).

administrated with iohexol to visualize the gastrointestinal tract profiles, benefiting the determination of the location of Bi_2S_3 capsules. For the control group, the capsules were mainly located in small intestinal before 8 h, and then moved into cecum and colon at about 8 h. The majority of capsules can be excreted from the body at 10 h. In contrast, for the vincristine-treated group, the movement speed of capsules slowed down obviously, and the majority of capsules were still located into small intestinal at 10 h due to the weakened gastrointestinal motility. While the metabolism of the capsules in gastrointestinal tract became normal after vincristine-treated rats were treated with AM251, as shown in the X-ray imaging. In addition, $BaSO_4$ capsules were also used to assess gastrointestinal motility in the rats with various treatments. However, the contrast effect of $BaSO_4$ capsules in X-ray imaging was much worse than that of Bi_2S_3 capsules, which demonstrated Bi_2S_3 can serve as an excellent alternative X-ray contrast agent to $BaSO_4$ (Fig. S17†).

Then we quantitatively assessed the gastrointestinal motility based on a standard rating scale (Table 1),[64,65] and two kinds of scores (total score and lead capsule score) were calculated for the assessment. The three capsules are given numerical scores based on their position in the gastrointestinal tract, and the total score is calculated by adding the score of each capsule (if all are excreted, the maximum is equal to 15). The lead capsule score was calculated based on its position in the gastrointestinal tract according to the rating scale (if it is excreted, the maximum is equal to 5). As shown in Fig. 6A, the average total scores of the vincristine group were 7.8 times at 4 h, 4.6 times at 8 h and 3.9 times at 10 h lower than those of the control group, respectively. After treated by AM251, the average total scores of vincristine & AM251 group increased by 4.8 times at 4 h, 3.2 times at 8 h and 2.8 times at 10 h compared with those of the VCR group, which indicated the gastrointestinal motility disorder caused by vincristine was significantly restored by AM251.

Besides, the lead capsule score was also used to evaluate the gastrointestinal motility. The lead capsules score of vincristine group were 2.4 times at 4 h, 2.7 times at 8 h, and 2.3 times at 10 h lower than those of the control group, respectively (Fig. 6B). The lead capsules in vincristine group only reached the distal small intestine area, while most of lead capsules in the control group were excreted at 10 h after oral administration. The lead capsules scores of vincristine & AM251 group were 1.6 times at 4 h, 2.3 times at 8 h and 2 times at 10 h higher than those of vincristine group. The lead capsules in the gastrointestinal tract were either in the descending colon or excreted at 10 h due to the recovery of gastrointestinal motility function.

Gastrointestinal transmission evaluation by CT and spectral CT imaging *in vivo*

Then the gastrointestinal motility assessment was evaluated by CT and spectral CT imaging using Bi_2S_3 capsules. The metabolism behavior of Bi_2S_3 capsules in the gastrointestinal tract of rats in various groups can be monitored in three dimensions clearly, providing more abundant diagnosis information. The gastrointestinal motility disorder and function recovery can be diagnosed by the visualized CT images and rating scores (Fig. S18 and S19†), and the results were consistent with those obtained from X-ray imaging. Besides, the spectral CT imaging

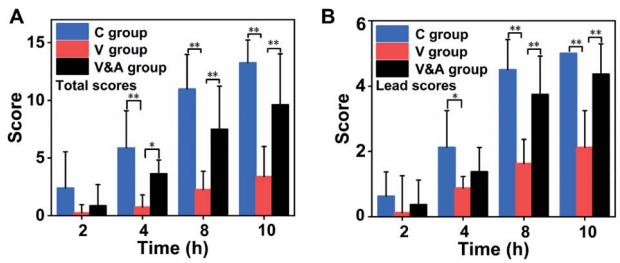

Fig. 6 The total scores (A) and lead capsule scores (B) of X-ray imaging of rats after various treatments at different time points. These data were shown as means ± SD, $n = 8$, evaluated by one-way analysis of variance, $*p < 0.05$, $**p < 0.01$.

Table 1 Bi_2S_3 capsule position score. Lead capsule refers to the most distally located capsule. Total score is determined by summing the scores of three capsules

Position	Stomach	Proximal small intestine	Distal small intestine
Score	0	1	2
Position	Cecum	Colon	Excretion of the gastrointestinal tract
Score	3	4	5

Open Access Article. Published on 05 May 2022. Downloaded on 3/3/2026 10:20:57 AM.
This article is licensed under a Creative Commons Attribution-NonCommercial 3.0 Unported Licence.

with the charming advantage of distinguishing the materials by different atomic numbers was also carried out (Fig. 7A–C and S20†). In common CT imaging or spectral CT imaging at low monochromatic energies, food, faeces, iohexol and other tissues all can be seen besides Bi_2S_3 capsules, and which resulted in troublesome interferences for the clear visualization of Bi_2S_3 capsules. While in spectral CT imaging at high monochromatic energies, the CT signal of other subjects decreased significantly, even disappeared. In contrast, Bi_2S_3 capsules still kept the constant strong brightness in spectral CT imaging regardless of the monochromatic energies, so the Bi_2S_3 capsules can be distinguished from the background very obviously at high monochromatic energies. Combined spectral CT imaging of Bi_2S_3 capsules at low and high monochromatic energies, the location information of Bi_2S_3 capsules and anatomical information of surrounding tissues can be obtained high sensitively and accurately. Therefore, the developed Bi_2S_3 capsules can serve as an excellent multifunctional X-ray contrast agent for gastrointestinal motility assessment based on X-ray, CT and spectral CT.

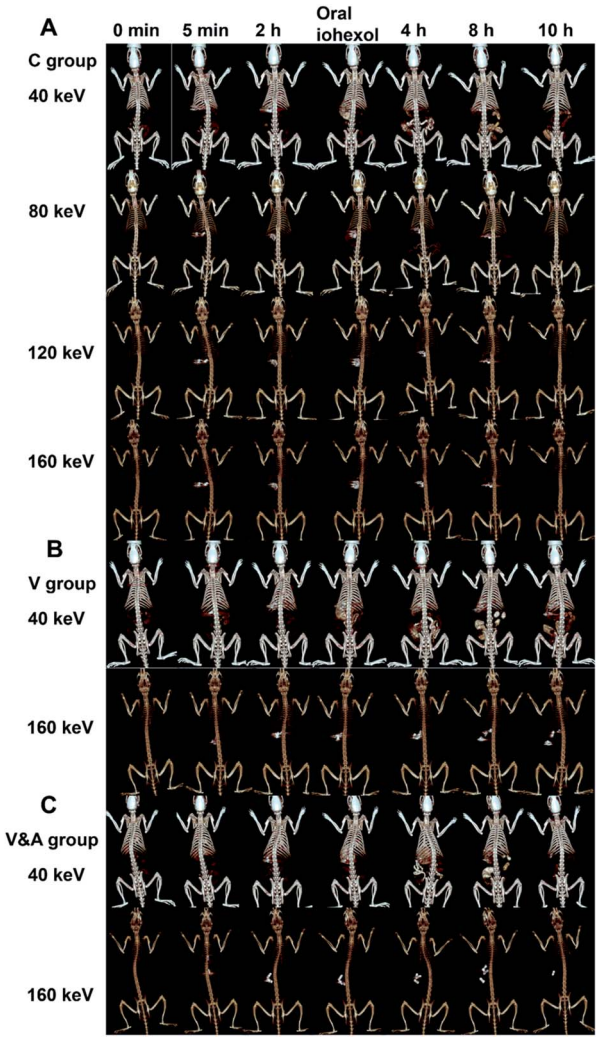

Fig. 7 Three-dimensional reconstructed images of rats under different monochromatic energies after various treatments at different time points (0 min, 5 min, 2 h, 4 h, 8 h, 10 h) *in vivo*. (A) Control group (C group), (B) vincristine-treated group (V group), (C) vincristine & AM251 treated group (V&A group).

Conclusions

In summary, we reported the facile fabrication of Bi_2S_3 capsules as a high-performance X-ray contrast agent for gastrointestinal motility assessment for the first time. Bi_2S_3 capsules were synthesized by encapsulating commercial Bi_2S_3 powder into gelatin capsules, followed by the coating of ultraviolet-curable resin. In the harsh environment of the gastrointestinal system, the synthesized Bi_2S_3 capsules can still keep intact morphology. The prepared Bi_2S_3 capsules showed superior X-ray absorption ability than $BaSO_4$ capsules at various conditions in X-ray and CT imaging *in vitro*. In particular, the large atomic number and high K-edge value of Bi ensure the outstanding contrast performance of Bi_2S_3 capsules at high monochromatic energies. The cellular studies proved the low cytotoxicity of Bi_2S_3 capsules, and the *in vivo* toxicity evaluation also confirmed the good biocompatibility of Bi_2S_3 capsules. Taking the vincristine-induced gastrointestinal motility disorder model as an example, the developed Bi_2S_3 capsules were successfully employed to quantitatively and sensitively assess gastrointestinal motility through X-ray, CT and spectral CT imaging *in vivo*, and the imaging performance of Bi_2S_3 capsules was much better than that of $BaSO_4$ capsules. Our study demonstrated the feasibility of a highly sensitive gastrointestinal motility assessment using a Bi-based contrast agent with great clinical translation potential, which can serve as an excellent alternative contrast agent to clinically used $BaSO_4$.

Author contributions

S.-K. Sun and X.-J. Zhang supervised the project. Y. Wen and W. Zhu performed the experiments. Y. Wen principally wrote the manuscript. All authors proof-read, provided comments, and approved the final version of this manuscript.

Conflicts of interest

The authors declare no competing financial interest.

Acknowledgements

This work was supported by the National Natural Science Foundation of China (21874101, 21934002, and 82071982) and the Natural Science Foundation of Tianjin City (19JCJQJC63700) and Young Elite Scientists Sponsorship Program by Tianjin (TJSQNTJ-2018-08).

Notes and references

1 R. M. McQuade, V. Stojanovska, R. Abalo, J. C. Bornstein and K. Nurgali, *Front. Pharmacol.*, 2016, **7**, 414.
2 P. Bytzer, N. J. Talley and M. Leemon, *Arch. Intern. Med.*, 2001, **161**, 1989–1996.

 © 2022 The Author(s). Published by the Royal Society of Chemistry

Open Access Article. Published on 05 May 2022. Downloaded on 3/3/2026 10:20:57 AM.
This article is licensed under a Creative Commons Attribution-NonCommercial 3.0 Unported Licence.

3 E. M. Richards, C. J. Pepine, M. K. Raizada and S. Kim, *Curr. Hypertens. Rep.*, 2017, **19**, 36.
4 X. Fu, Z. Li, Z. Na, H. Yu and J. Liu, *Nutr. Metab.*, 2014, **11**, 3.
5 B. M. Yeh, P. F. FitzGerald, P. M. Edic, J. W. Lambert, R. E. Colborn, M. E. Marino, P. M. Evans, J. C. Roberts, Z. J. Wang, M. J. Wong and P. J. Bonitatibus Jr, *Adv. Drug Delivery Rev.*, 2017, **113**, 201–222.
6 E. M. Lavoie Smith, D. L. Barton, R. Qin, P. D. Steen, N. K. Aaronson and C. L. Loprinzi, *Qual. Life Res.*, 2013, **22**, 2787–2799.
7 E. Y. Ibrahim and B. E. Ehrlich, *Crit. Rev. Oncol. Hematol.*, 2020, **145**, 102831.
8 S. B. Park, D. Goldstein, A. V. Krishnan, C. S. Y. Lin, M. L. Friedlander, J. Cassidy, M. Koltzenburg and M. C. Kiernan, *Ca-Cancer J. Clin.*, 2013, **63**, 419–437.
9 B. W. Hancock and A. Naysmith, *Br. Med. J.*, 1975, **3**, 207.
10 S. Dudeja, S. Gupta, S. Sharma, A. Jain, S. Sharma, P. Jain, S. Aneja and J. Chandra, *Pediatr. Hematol. Oncol.*, 2019, **36**, 344–351.
11 S. Quasthoff and H. P. Hartung, *J. Neurol.*, 2002, **249**, 9–17.
12 E. R. Kim and P. L. Rhee, *J. Neurogastroenterol. Motil.*, 2012, **18**, 94–99.
13 J. T. Fell and G. A. Digenis, *Int. J. Pharm.*, 1984, **22**, 1–15.
14 R. M. McQuade, V. Stojanovska, R. Abalo, J. C. Bornstein and K. Nurgali, in *Colonic Transit Study by Radio-Opaque Markers*, Springer, New Delhi, 2016, pp. 23–29.
15 H. Sharif, N. Abrehart, C. L. Hoad, K. Murray, A. C. Perkins, M. Smith, P. A. Gowland, R. C. Spiller, R. Harris, S. Kirkham, S. Loganathan, M. Papadopoulos, K. Frost, D. Devadason, L. Marciani and G. Young Persons Advisory, *J. Pediatr. Gastroenterol. Nutr.*, 2020, **71**, 604–611.
16 R. B. Kjeldsen, M. N. Kristensen, C. Gundlach, L. H. E. Thamdrup, A. Mullertz, T. Rades, L. H. Nielsen, K. Zor and A. Boisen, *ACS Biomater. Sci. Eng.*, 2021, **7**, 2538–2547.
17 A. Jakhmola, N. Anton and T. F. Vandamme, *Adv. Healthcare Mater.*, 2012, **1**, 413–431.
18 R. Bomma, R. A. S. Naidu, M. R. Yamsani and K. Veerabrahma, *Acta Pharm.*, 2009, **59**, 211–221.
19 A. S. Narang, A. Balakrishnan, J. Morrison, J. Li, J. Wang, H. Gu, K. Taylor, K. Santone, J. Ehrmann, S. Beyer, X. Lu, R. Ketner, J. Pizzano, T. Orcutt, E. Shields, H. Dulac, S. Aborn, M. Batchelder and K. Lentz, *Eur. J. Pharm. Biopharm.*, 2017, **117**, 333–345.
20 K. Kikuchi, M. Kusano and O. Kawamura, *Dig. Dis. Sci.*, 2000, **45**, 242–247.
21 S. Saphier, A. Rosner, R. Brandeis and Y. Karton, *Int. J. Pharm.*, 2010, **388**, 190–195.
22 Y. B. Wang, G. Li, Y. F. Wang, Y. J. Ding, G. Z. Yan, D. Han, Z. W. Wang and X. H. Zhao, *Int. J. Colorectal Dis.*, 2020, **35**, 29–34.
23 S. S. Rao, K. Rattanakovit and T. Patcharatrakul, *Nat. Rev. Gastroenterol. Hepatol.*, 2016, **13**, 295–305.
24 H. C. Lin, C. Prather, R. S. Fisher, J. H. Meyer, R. W. Summers, M. Pimentel, R. W. McCallum, L. M. Akkermans and V. Loening-Baucke, *Dig. Dis. Sci.*, 2005, **50**, 989–1004.
25 S. S. Rao, M. Camilleri, W. L. Hasler, A. H. Maurer, H. P. Parkman, R. Saad, M. S. Scott, M. Simren, E. Soffer and L. Szarka, *Neurogastroenterol. Motil.*, 2011, **23**, 8–23.
26 P. C. Naha, J. C. Hsu, J. Kim, S. Shah, M. Bouche, S. Si-Mohamed, D. N. Rosario-Berrios, P. Douek, M. Hajfathalian, P. Yasini, S. Singh, M. A. Rosen, M. A. Morgan and D. P. Cormode, *ACS Nano*, 2020, **14**, 10187–10197.
27 N. Lee, S. H. Choi and T. Hyeon, *Adv. Mater.*, 2013, **25**, 2641–2660.
28 Y. Zu, Y. Yong, X. Zhang, J. Yu, X. Dong, W. Yin, L. Yan, F. Zhao, Z. Gu and Y. Zhao, *RSC Adv.*, 2017, **7**, 17505–17513.
29 T. M. Coupal, P. I. Mallinson, S. L. Gershony, P. D. McLaughlin, P. L. Munk, S. Nicolaou and H. A. Ouellette, *Am. J. Roentgenol.*, 2016, **206**, 119–128.
30 X. F. Luo, X. Q. Xie, S. Cheng, Y. Yang, J. Yan, H. Zhang, W. M. Chai, B. Schmidt and F. H. Yan, *Radiology*, 2015, **277**, 95–103.
31 A. N. Primak, J. G. Fletcher, T. J. Vrtiska, O. P. Dzyubak, J. C. Lieske, M. E. Jackson, J. C. Williams Jr and C. H. McCollough, *Acad. Radiol.*, 2007, **14**, 1441–1447.
32 E. Pessis, R. Campagna and J. M. Sverzut, *RadioGraphics*, 2013, **33**(2), 573–583.
33 Y. Y. Jin, D. L. Ni, L. Gao, X. F. Meng, Y. Lv, F. Han, H. Zhang, Y. Y. Liu, Z. W. Yao, X. Y. Feng, W. B. Bu and J. W. Zhang, *Adv. Funct. Mater.*, 2018, **28**, 1802656.
34 Y. L. Liu, K. L. Ai, J. H. Liu, Q. H. Yuan, Y. Y. He and L. H. Lu, *Angew. Chem., Int. Ed.*, 2012, **51**, 1437–1442.
35 D. Pan, E. Roessl, J.-P. Schlomka, S. D. Caruthers, A. Senpan, M. J. Scott, J. S. Allen, H. Zhang, G. Hu, P. J. Gaffney, E. T. Choi, V. Rasche, S. A. Wickline, R. Proksa and G. M. Lanza, *Angew. Chem., Int. Ed.*, 2010, **49**, 9635–9639.
36 H. Li and H. Sun, *Curr. Opin. Chem. Biol.*, 2012, **16**, 74–83.
37 Y. Cheng and H. Zhang, *Chem.–Eur. J.*, 2018, **24**, 17405–17418.
38 Y. Xuan, X. Q. Yang, Z. Y. Song, R. Y. Zhang, D. H. Zhao, X. L. Hou, X. L. Song, B. Liu, Y. D. Zhao and W. Chen, *Adv. Funct. Mater.*, 2019, **29**, 1900017.
39 M. A. Shahbazi, L. Faghfouri, M. P. A. Ferreira, P. Figueiredo, H. Maleki, F. Sefat, J. Hirvonen and H. A. Santos, *Chem. Soc. Rev.*, 2020, **49**, 1253–1321.
40 X. Zheng, J. Shi, Y. Bu, G. Tian, X. Zhang, W. Yin, B. Gao, Z. Yang, Z. Hu, X. Liu, L. Yan, Z. Gu and Y. Zhao, *Nanoscale*, 2015, **7**, 12581–12591.
41 K. D. Mjos and C. Orvig, *Chem. Rev.*, 2014, **114**, 4540–4563.
42 S. L. Gorbach, *Gastroenterology*, 1990, **99**, 863–875.
43 D. M. Keogan and D. M. Griffith, *Molecules*, 2014, **19**, 15258–15297.
44 B. Wei, X. Zhang, C. Zhang, Y. Jiang, Y. Y. Fu, C. Yu, S. K. Sun and X. P. Yan, *ACS Appl. Mater. Interfaces*, 2016, **8**, 12720–12726.
45 N. Yu, Z. Wang, J. Zhang, Z. Liu, B. Zhu, J. Yu, M. Zhu, C. Peng and Z. Chen, *Biomaterials*, 2018, **161**, 279–291.
46 P. Lei, R. An, P. Zhang, S. Yao, S. Song, L. Dong, X. Xu, K. Du, J. Feng and H. Zhang, *Adv. Funct. Mater.*, 2017, **27**, 1702018.
47 X. Yu, A. Li, C. Zhao, K. Yang, X. Chen and W. Li, *ACS Nano*, 2017, **11**, 3990–4001.

Open Access Article. Published on 05 May 2022. Downloaded on 3/3/2026 10:20:57 AM.
This article is licensed under a Creative Commons Attribution-NonCommercial 3.0 Unported Licence.

48 F. Du, J. Lou, R. Jiang, Z. Fang, X. Zhao, Y. Niu, S. Zou, M. Zhang, A. Gong and C. Wu, *Int. J. Nanomed.*, 2017, **12**, 5973–5992.
49 H. Aviv, S. Bartling, I. Grinberg and S. Margel, *J. Biomed. Mater. Res., Part B*, 2013, **101**, 131–138.
50 Y. Xujiang, L. Xinyi, Y. Kai, C. Xiaoyuan and L. Wanwan, *ACS Nano*, 2021, **15**, 2038–2067.
51 W. Xu, P. Cui, E. Happonen, J. Leppanen, L. Liu, J. Rantanen, D. Majda, A. Saukko, R. Thapa, T. Nissinen, T. Tynkkynen, J. Toyras, L. Fan, W. Liu and V. P. Lehto, *ACS Appl. Mater. Interfaces*, 2020, **12**, 47233–47244.
52 F. Mao, L. Wen, C. Sun, S. Zhang, G. Wang, J. Zeng, Y. Wang, J. Ma, M. Gao and Z. Li, *ACS Nano*, 2016, **10**, 11145–11155.
53 X. Niu, Y. Liu, X. Li, W. Wang and Z. Yuan, *Adv. Funct. Mater.*, 2020, **30**, 2006883.
54 X.-D. Zhang, J. Chen, Y. Min, G. B. Park, X. Shen, S.-S. Song, Y.-M. Sun, H. Wang, W. Long, J. Xie, K. Gao, L. Zhang, S. Fan, F. Fan and U. Jeong, *Adv. Funct. Mater.*, 2014, **24**, 1718–1729.
55 L. Li, Y. Lu, C. Jiang, Y. Zhu, X. Yang, X. Hu, Z. Lin, Y. Zhang, M. Peng, H. Xia and C. Mao, *Adv. Funct. Mater.*, 2018, **28**, 1704623.
56 Y. Wang, Y. Wu, Y. Liu, J. Shen, L. Lv, L. Li, L. Yang, J. Zeng, Y. Wang, L. W. Zhang, Z. Li, M. Gao and Z. Chai, *Adv. Funct. Mater.*, 2016, **26**, 5335–5344.
57 K. Ai, Y. Liu, J. Liu, Q. Yuan, Y. He and L. Lu, *Adv. Mater.*, 2011, **23**, 4886–4891.
58 O. Rabin, J. Manuel Perez, J. Grimm, G. Wojtkiewicz and R. Weissleder, *Nat. Mater.*, 2006, **5**, 118–122.
59 D. Wang, C. Hao, W. Zheng, X. Ma, D. Chu, Q. Peng and Y. Li, *Nano Res.*, 2010, **2**, 130–134.
60 J. Arumugam, A. D. Raj, A. A. Irudayaraj and M. Thambidurai, *Mater. Lett.*, 2018, **220**, 28–31.
61 S. Ding, A. I. Khan, X. Cai, Y. Song, Z. Lyu, D. Du, P. Dutta and Y. Lin, *Mater. Today*, 2020, **37**, 112–125.
62 A. B. Bello, D. Kim, D. Kim, H. Park and S.-H. Lee, *Tissue Eng., Part B*, 2020, **26**, 164–180.
63 G. Vera, A. E. Lopez-Perez, J. A. Uranga, R. Giron, M. I. Martin-Fontelles and R. Abalo, *Front. Pharmacol.*, 2017, **8**, 37.
64 J. E. Dalziel, W. Young, P. Bercik, N. J. Spencer, L. J. Ryan, K. E. Dunstan, C. M. Lloyd-West, P. K. Gopal, N. W. Haggarty and N. C. Roy, *Neurogastroenterol. Motil.*, 2016, **28**, 1241–1251.
65 D. E. Reed, M. Pigrau, J. Lu, P. Moayyedi, S. M. Collins and P. Bercik, *Neurogastroenterol. Motil.*, 2014, **26**, 1663–1668.

 © 2022 The Author(s). Published by the Royal Society of Chemistry